JCTC Journal of Chemical Theory and Computation

Article

pubs.acs.org/JCTC

Understanding the ε and ζ High-Pressure Solid Phases of Oxygen. Systematic Periodic Density Functional Theory Studies Using Localized Atomic Basis

A. J. Ochoa-Calle,[†] C. M. Zicovich-Wilson,[†] R. Hernández-Lamoneda,[‡] and A. Ramírez-Solís*[,†]

[†]Departamento de Física, Centro de Investigación en Ciencias, Universidad Autónoma del Estado de Morelos, Av. Universidad 1001, Cuernavaca, Morelos 62209, México

[‡]Centro de Investigaciones Químicas, Universidad Autónoma del Estado de Morelos, Av. Universidad 1001, Cuernavaca, Morelos 62209, México

ABSTRACT: The experimentally characterized ε and ζ phases of solid oxygen are studied by periodic Hartree−Fock (HF) and Density Functional Theory calculations at pressures from 10 to 160 GPa using different types of exchange-correlation functionals with Gaussian atomic basis sets. Full geometry optimizations of the monoclinic $C2/m$ $(O_2)_4$ unit cell were done to study the evolution of the structural and electronic properties with pressure. Vibrational calculations were performed at each pressure. While periodic HF does not predict the $\varepsilon-\zeta$ phase transition in the considered range, Local Density approximation and Generalized Gradient approximation methods predict too low transition pressures. The performance of hybrid functional methods is dependent on the amount of non-local HF exchange. PBE0, M06, B3PW91, and B3LYP approaches correctly predict the structural and electronic changes associated with the phase transition. GGA and hybrid functionals predict a pressure range where both phases coexist, but only the latter type of methods yield results in agreement with experiment. Using the optimized $(O_2)_4$ unit cell at each pressure we show, through CASSCF(8,8) calculations, that the greater accuracy of the optimized geometrical parameters with increasing pressure is due to a decreasing multireference character of the unit cell wave function. The mechanism of the transition from the non-conducting to the conducting ζ phase is explained through the Electron Pair Localization Function, which clearly reveals chemical bonding between O_2 molecules in the *ab* crystal planes belonging to different unit cells due to much shorter intercell O_2-O_2 distances.

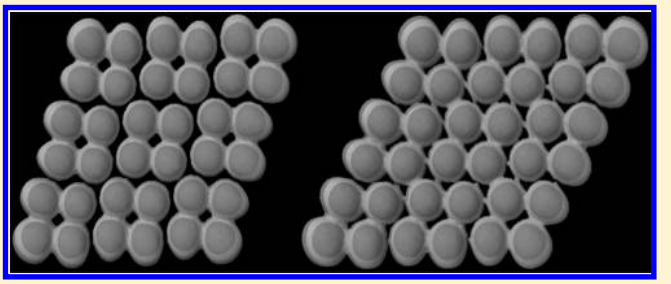

I. INTRODUCTION

The solid phases of oxygen have been investigated for over a century using many experimental techniques. The evolution of their physical properties with pressure has come to be a fascinating topic, and a plethora of studies have provided precise quantitative knowledge about their structural, energetic, optical, and magnetic properties. The complex phase diagram for solid oxygen vs pressure shows a large number of different phases, all of them arising from oxygen diatomic molecules arranged in various geometrical configurations. It is interesting to note that these phases can be strikingly different, in particular concerning their color, unit cell volume, and magnetic properties. Freiman and Jodl[1] published a comprehensive review of what is known concerning all the phases of solid oxygen and provided relevant experimental and theoretical references. It is now clear that the changes in these properties are due to the specific way in which the diatomic molecules interact in each type of unit cell as pressure increases. The exchange interaction between the O_2 molecules in solid oxygen acts on the background of weak van der Waals forces and provides a significant amount of the total lattice energy. At low temperatures or under high pressure, molecular oxygen becomes first, a paramagnetic liquid, then a solid by the action of weak intermolecular forces. At low pressure oxygen transforms into monoclinic α-O_2 through γ- and β-O_2 by cooling. At higher pressures it is known that α-O_2 transforms to ε-O_2 directly at 7.2 GPa and 19 K.[2] While the transition of the non-magnetic solid ε-O_2 to the conducting ζ-O_2 phase was discovered in 1995,[3] but the true nature of their unit cells was unknown until 2006. Only recently it has been possible to perform very accurate studies for solid oxygen under high pressures using X-ray diffraction experiments with high-brilliance synchrotron radiation.[4,5] These nearly simultaneous experiments led their authors to the same conclusion: the ε and ζ phases are isosymmetric within the $C2/m$ lattice group and their unit cells consist of $(O_2)_4$ clusters. The ε phase transforms into the metallic ζ phase at 96 GPa which becomes a superconducting state at 0.6 K. Interestingly, ζ-O_2 becomes the only known molecular superconductor at temperatures below 0.6 K.[6] However, it is important to highlight that the ε and ζ phases coexist in a pressure range going from 96 to 110 GPa.[7] Also reliable experimental information exists concerning the evolution of the optical vibron (the all-in-phase stretching

Received: January 8, 2015

DOI: 10.1021/acs.jctc.5b00017
J. Chem. Theory Comput. XXXX, XXX, XXX−XXX

vibrational mode of the four O_2 molecules in the unit cell) in the 10−120 GPa pressure range,[8] but this issue will be theoretically addressed elsewhere in the near future.

The crystalline structure of these high-pressure oxygen phases has been studied from the theoretical perspective. Density Functional theory (DFT) calculations using the local density approximation (LDA) were first considered to obtain the structure of the ε and ζ phases.[9] However, the predicted LDA structure for the non-magnetic ε-O_2 phase is not consistent with experimental data since the local density approximation cannot properly describe the weak magnetic interaction between oxygen molecules. Therefore, several more refined theoretical attempts have been made through periodic studies employing the Generalized Gradient approximation (GGA) with plane wave basis sets.[10−13] Nevertheless, in spite of using more refined semilocal density functionals, the GGA calculations of Neaton et al.[10] and of Oganov et al.[11] wrongly predicted O_2−O_2 zigzag chains as unit cell for the ε-O_2 phase.

We point out that Ma et al.[12] reported the first theoretical study concerning the ζ phase. An important result obtained by Militzer and Hemley[14] is that these optimized O_2−O_2 chains have a lower enthalpy than the experimental $(O_2)_4$ ε phase unit cell at that level of theory, thus these authors highlighted the need of more refined theoretical studies. Note also that previous GGA-GW studies on the phase transition[13] wrongly predicted the ε−ζ lattice changes and the band gap collapse at rather low pressures ca. 50 GPa. As we shall see, the failure of these methods can be traced back, at least partially, to the difficulty in accurately describing the long-range exchange interactions with GGA-type methods.

We note that it is possible to perform periodic electronic structure calculations of solids efficiently using hybrid functionals (containing a fraction of the non-local Hartree−Fock exchange) in conjunction with localized atomic basis sets.[15] This more refined approach to deal with complex non-local effects where exchange interactions are crucial to determine the most stable crystalline structure has been successfully applied in many cases (see, for instance, ref 16). In this context, the goals of this investigation are 2-fold. First, since previous theoretical attempts at describing the ε−ζ phase transition have not been successful, we aim at finding if a quantum theoretical approach exists that correctly reproduces the structural XRD data of solid oxygen vs pressure. Therefore, we report a systematic study of the evolution of structural and electronic properties of the solid ε and ζ phases using periodic Hartree−Fock and DFT with localized Gaussian atomic basis sets. Within the DFT scheme we consider several exchange-correlation density functionals from the LDA, GGA, meta-GGA, and the hybrid functional types. This systematic study allows us to extract insights and conclusions concerning the relative quality of each type of description as we climb from the simplest to the most sophisticated types of density functionals. If at least one of the more refined methods turns out to be successful in correctly describing the structural and energetic features of solid oxygen at high pressures, our second (non-methodological) goal is to identify the nature of the electronic changes that are at the root of the non-conducting to conducting phase transition by studying the variation of the band structure (in particular the band gap) vs pressure for both phases. These electronic changes will be discussed in light of the changes of intermolecular distances and the amount of opposite-spin electron pairing between same-cell and different-cell O_2 molecules as a function of pressure. For obvious reasons we will focus on the structural and electronic properties of both phases around the experimental transition pressure. The quality of the energetic and structural description provided by these more refined functionals will be ascertained through the comparison of theoretical results with the XRD and Raman spectroscopic data. In light of the fact that only single-reference type quantum chemical descriptions can be done for solid oxygen, a careful discussion is presented in section III, where detailed aspects of the complexity of the electronic structure problem of the $(O_2)_4$ unit cell are discussed. As it will be shown, the relative quality of the structural predictions at low and high pressures is directly related to the multireference vs single-reference character of the lowest-spin unit cell wave function. Finally, we present a global assessment of the study along with general conclusions and future perspectives, both from the methodological and the material science stances.

II. METHOD: PERIODIC HARTREE−FOCK AND DFT CALCULATIONS

In order to study the evolution of the geometrical parameters of the solid oxygen phases as a function of pressure we have considered periodic HF and DFT within the local density approximation (LDA[17]), using four GGA-type (BLYP,[18,19] PBE,[20] SOGGAXC,[21] B88PW91[18,22]), one meta-GGA type (M06-L[23]), and four hybrid exchange-correlation functionals (PBE0,[24] M06,[25] B3PW91,[26,22] and B3LYP[26,19]) in conjunction with the Ahlrichs triple-ζ plus polarization Gaussian atomic basis set for oxygen.[27] The periodic HF and DFT calculations were done with the CRYSTAL14 code[15] which, at variance with previous studies, allows enthalpy-driven geometry optimizations with a fixed hydrostatic pressure imposed on the boundaries of the unit cell. Full geometry optimizations were done with analytical gradients for the unit cell and internal atomic parameters, while retaining the experimentally determined symmetry of these high pressure phases. Convergence criteria for geometry optimization were as follows: maximum energy gradient/component = 0.00045, RMS energy gradient/component = 0.0003, maximum displacement/component = 0.0018, RMS displacement/component = 0.0012, and energy convergence threshold = 10^{-8}, all in a.u.

Since detailed XRD information is available for the solid ε phase, we used as an initial guess at 10 GPa the atomic coordinates from ref 5 and the $C2/m$ crystalline group to perform the geometry optimizations of this phase. The unit cell of both phases is composed of four oxygen molecules,[5,7] so the DFT calculations involve 160 crystal orbitals per k-point and seven symmetry-allowed degrees of freedom. Figure 1 shows the unit cell geometry.

Experiments have shown that these phases are non-magnetic; therefore, we have followed the lowest Kohn−Sham solution whose total spin is zero for each pressure. The studied pressure range was 10 to 160 GPa with incremental steps of 10 GPa and smaller increments (2 to 5 GPa) around the transition pressures predicted by each method. In order to find the coexistence pressure range of both phases, once convergence was achieved to the ζ phase at a functional-dependent pressure P_{high}, we used the optimized geometry and density matrix to perform a new set of geometry optimizations of this phase to lower pressures. This strategy favors continuity of the solutions along the series. This pressure-decreasing process ended when the ζ phase collapsed back to the ε phase at a functional-dependent pressure P_{low}. Except for the symmetry restriction noted above, the lattice parameters as well as atomic positions

DOI: 10.1021/acs.jctc.5b00017
J. Chem. Theory Comput. XXXX, XXX, XXX−XXX

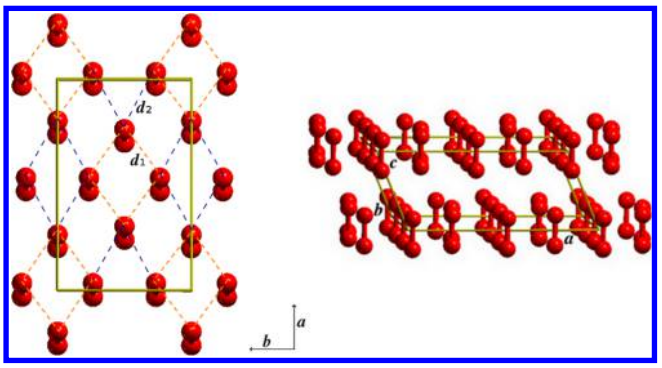

Figure 1. Unit cell of the ε and ζ phases of solid oxygen in the $C2/m$ crystal group. The intermolecular d_1 (intracell) and d_2 (intercell) distances as well as the monoclinic angle β are shown.

were completely optimized at each pressure. The reciprocal space was sampled using 150 k-points (a 8 × 8 × 8 Monkhorst net) in the Brillouin zone, and the Broyden scheme[28,29] was used to accelerate SCF convergence. A smearing factor of 0.0005 was used for the SCF convergence of the conducting state of the ζ phase, and, for the sake of consistency, the same approach was employed for the ε phase. Concerning the periodic integral accuracy, the {8, 7, 7, 9, 24} set of integral tolerances (see Crystal code manual, ref 15) has been employed to determine the optimized geometrical parameters and their evolution with pressure for both phases. The ensemble of geometry optimizations and frequency calculations for the whole range of pressures at the various levels of theory was achieved in ca. 6 CPU months on 128 processors.

III. RESULTS AND DISCUSSION

A. The Electronic Structure Problem for the Unit Cell of the Solid ε Phase. Kohn−Sham DFT, a single-determinant based method, is routinely used to study many types of crystalline materials. However, the oxygen ε phase unit cell is known to be composed of four oxygen molecules which, in principle, have two open shells (degenerate π_g orbitals). This leads to five possible spin states (S = 0,1,2,3,4) for the $(O_2)_4$ unit cell. Since experiments showed that the ε phase is nonmagnetic, only the case of zero spin is relevant at high pressures. As mentioned above, it is now well-known that DFT calculations within the LDA or GGA schemes cannot reproduce the correct intermolecular interactions of oxygen molecules and yield both, wrong structural predictions for solid oxygen under pressure and wrong (too low) ε−ζ transition pressures. In the unit cells of the ε and ζ phases, both the HOMO and LUMO of the interacting oxygen molecules originate, asymptotically, from the π_g orbitals of the four isolated O_2 molecules. Thus, the DFT underestimation of the HOMO−LUMO gap causes a serious overestimation of the exchange energy. However, at very high pressures, the O_2 molecules come much closer to each other, and the dominant exchange interactions at larger O_2−O_2 distances are overcome at shorter distances by the electronic interactions appearing in regions where actual chemical bonding between the constituent molecules starts to appear. Accurate quantum chemical

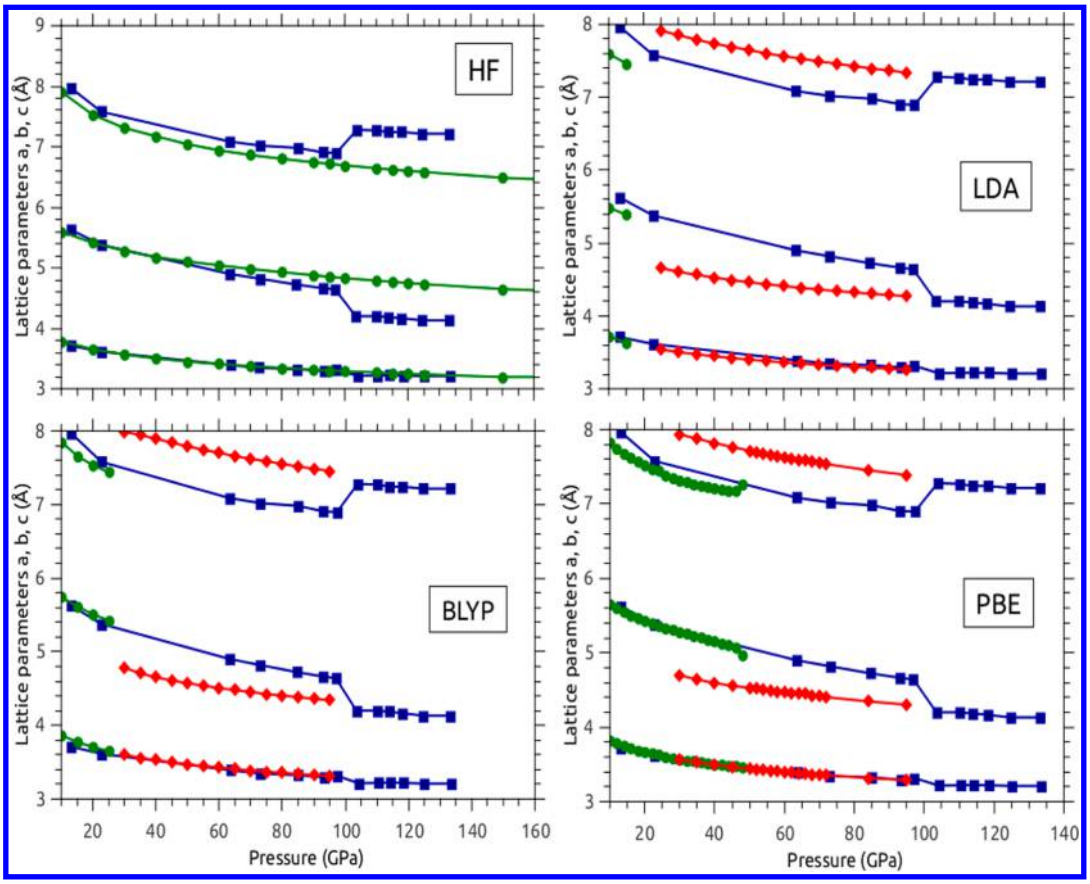

Figure 2. Optimized **a** (top curves), **b** (middle curves), and **c** (bottom curves) unit cell parameters at the HF, LDA, BLYP, and PBE levels. ε data (green), ζ data (red), and experimental results in blue from ref 7.

DOI: 10.1021/acs.jctc.5b00017
J. Chem. Theory Comput. XXXX, XXX, XXX−XXX

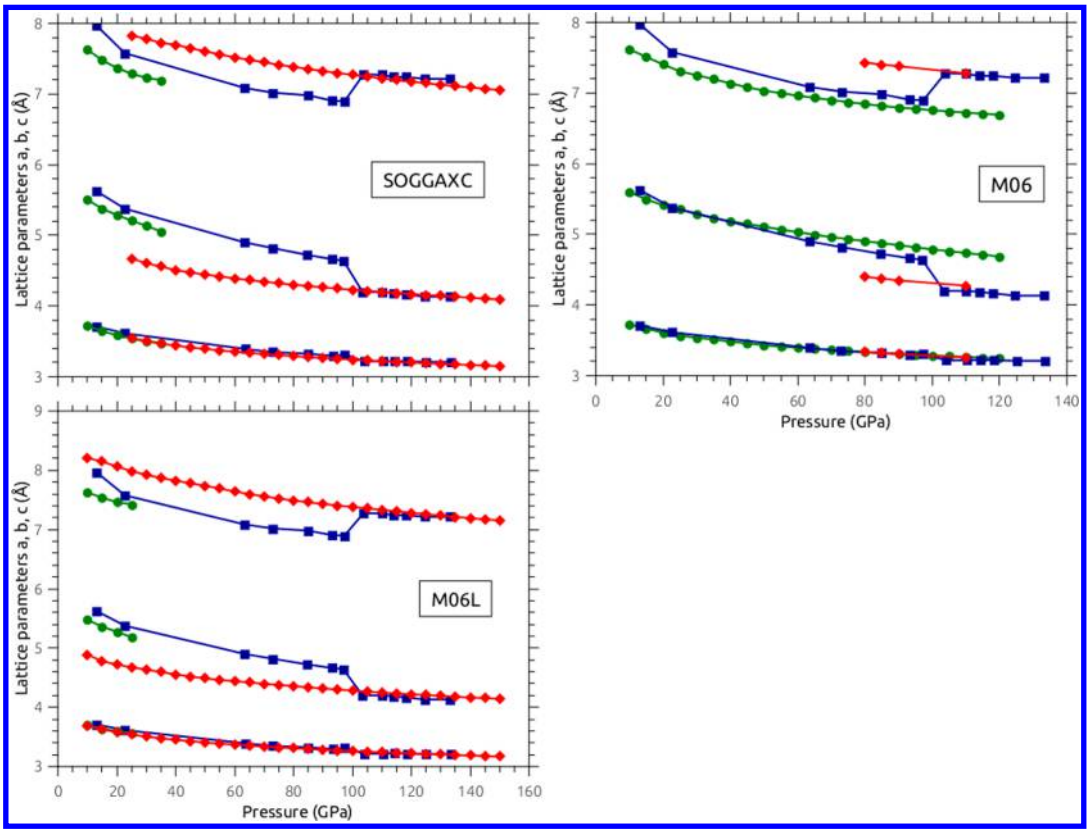

Figure 3. Optimized **a** (top curves), **b** (middle curves), and **c** (bottom curves) unit cell parameters at the SOGGAXC, M06, and M06-L levels. ϵ data (green), ζ data (red), and experimental results in blue from ref 7.

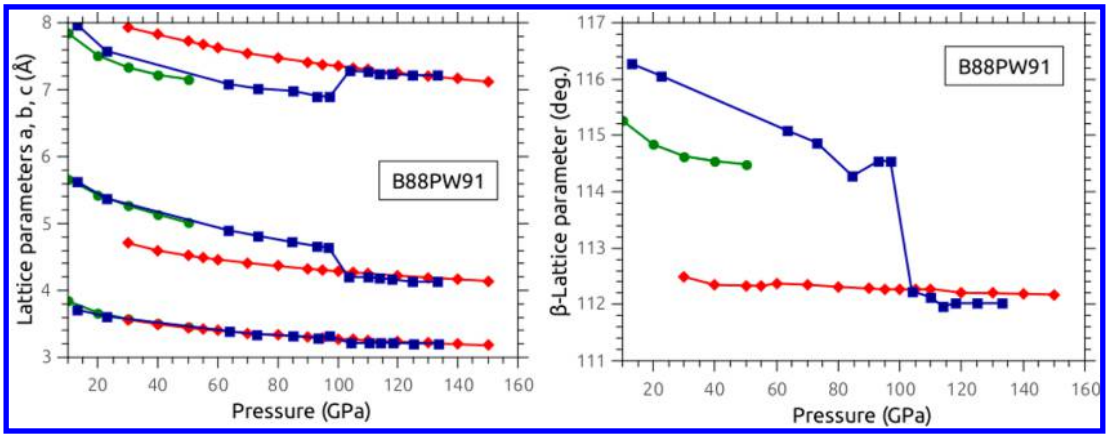

Figure 4. Optimized **a**, **b**, and **c** and β unit cell parameters at the GGA-B88PW91 level. ϵ data (green), ζ data (red), and experimental results in blue from ref 7.

calculations of the O_2 tetramer have been reported in relation to the solid ϵ phase,[30,31] where multiconfigurational *ab initio* calculations were used for the singlet ground state of $(O_2)_4$, which is compatible with the non-magnetic ϵ phase of $C2/m$ lattice symmetry. It was found that the cuboid $(O_2)_4$ structure is a van der Waals-like cluster where exchange interactions preferentially stabilize the singlet state. Nevertheless, as the cluster shrinks, there is an extra stabilization due to many-body interactions, i.e., an incipient chemical bonding that results in a slight softening of the repulsive wall between the O_2 molecules ca. 2.1 Å. These findings were used to successfully model the intra- and intercluster distances of ϵ-O_2.[30] The performance of different density functionals within the same simplified structural model has also been reported.[32] Using quantum chemical topological descriptors a significant spin redistribution was found for the O_2 tetramer as a function of the intermolecular distance, showing evidence of the transformation from antiferromagnetic coupling to a complete spin pairing process leading to a null magnetic moment.[31] We shall further discuss the fundamental electronic structure problem in $(O_2)_4$ when we analyze the evolution of the optimized DFT unit cell structures vs pressure.

B. Structural Evolution with Pressure and the ϵ–ζ Phase Transition. Starting from the lattice parameters reported at 17.5 GPa in ref 5, the geometry optimization at each pressure required 15–25 steps. As done in the previous theoretical studies of solid oxygen, the ϵ–ζ phase transition pressure was determined as that where the optimized a (and b)

DOI: 10.1021/acs.jctc.5b00017
J. Chem. Theory Comput. XXXX, XXX, XXX–XXX

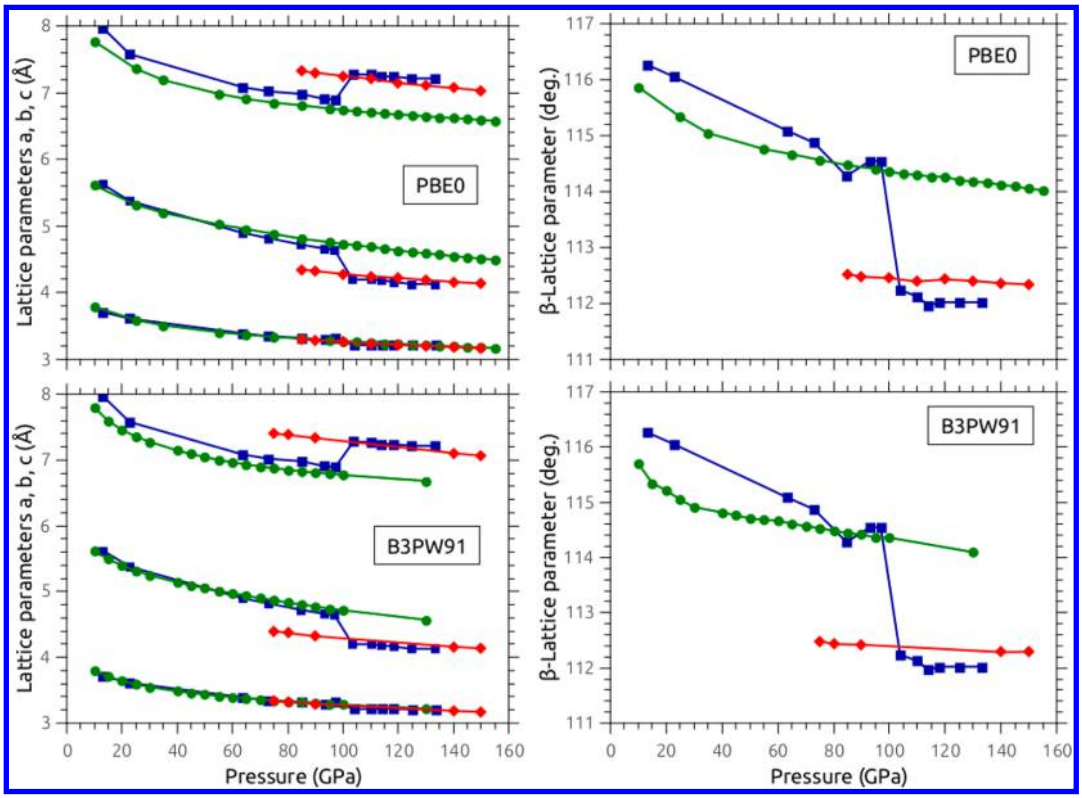

Figure 5. Optimized **a**, **b**, and **c** and β unit cell parameters at the PBE0 and B3PW91 levels. ϵ data (green), ζ data (red), and experimental results in blue from ref 7.

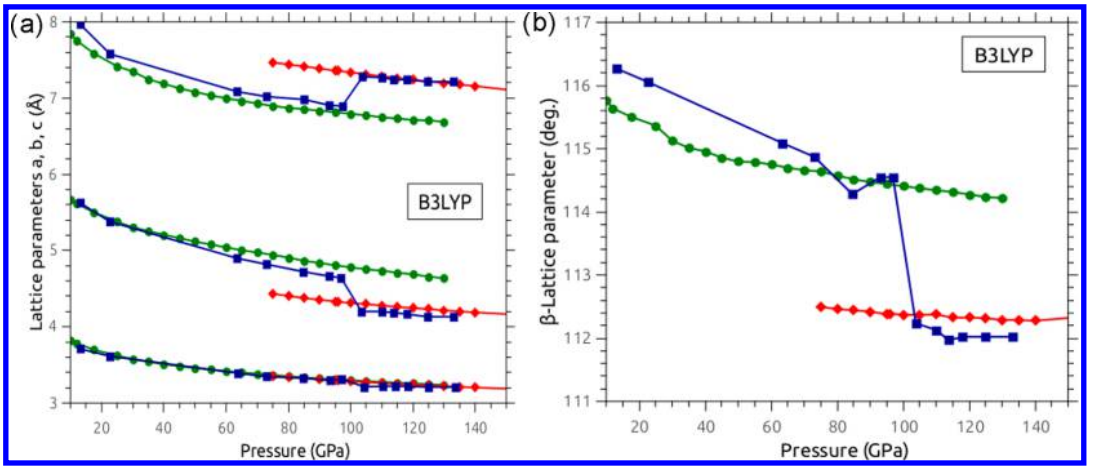

Figure 6. Optimized B3LYP **a**, **b**, and **c** unit cell parameters (a) and β angle (b) as a function of pressure. Note the phase coexistence in the 75−135 GPa pressure range. ϵ data (green), ζ data (red), and experimental results in blue from ref 7.

lattice parameters show a discontinuous increase (decrease) with respect to the previous lower pressure. Experimentally, the phase transition also involves a sudden decrease of the monoclinic angle β at the transition pressure.[4,7] At variance with previous studies, we find that, except for the periodic Hartree−Fock, LDA, and BLYP, all other methods predict a large ϵ/ζ phase coexistence pressure range. However, PBE0, B3PW91, and B3LYP yield transition pressures closer to the experimental value of 95 GPa, a fact which led us to study in greater detail the structural description of solid oxygen provided by these methods. Actually, through the pressure-decreasing optimization scheme detailed in section II, starting from the ζ phase at 135 GPa, we discovered that the B3LYP and B3PW91 methods yield a hysteresis-like behavior vs pressure of the optimized geometrical parameters. Indeed, these hybrid B3 exchange-based functionals predict two sets of stable unit cell structures for pressures going from 75 to 135 GPa for B3LYP and from 75 to 145 GPa for B3PW91, implying phase coexistence ranges. Once these results were found, it seemed quite odd that through the pressure-increasing optimization scheme the other hybrid methods (PBE0 and M06) did not predict the $\epsilon-\zeta$ phase transition; therefore, for these methods we decided to use as a starting point the optimized B3LYP geometry and density matrix to perform geometry optimizations at 110 GPa (this being the experimental high-pressure phase coexistence limit). As expected, using this approach we found that these hybrid methods also predict phase coexistence pressure ranges. We extended this pressure-decreasing

DOI: 10.1021/acs.jctc.5b00017
J. Chem. Theory Comput. XXXX, XXX, XXX−XXX

optimization scheme to the GGA methods and found that phase coexistence is also predicted by some of these less sophisticated approaches, although the corresponding phase coexistence pressure ranges are too low compared to the 95−110 GPa experimental one. Figures 2−7 show the evolution of the lattice parameters vs pressure for a representative set of methods used here.

Since the structural and energetic descriptions provided by PBE0, B3LYP, and B3PW91 are very similar, we focus here on the B3LYP results. The geometries of the first set of unit cells are in close agreement with the experimental data of the ε phase, while the second set having a slightly higher enthalpy at each pressure (discussed in detail below), is in very good agreement with the experimental unit cell parameters of the ζ phase. The evolution of the optimized B3LYP unit cell parameters are shown vs experimental data for varying pressure in Figure 6.

Figure 7 shows the good agreement of the predicted B3LYP d_1 (intracell) and d_2 (intercell) intermolecular distances with

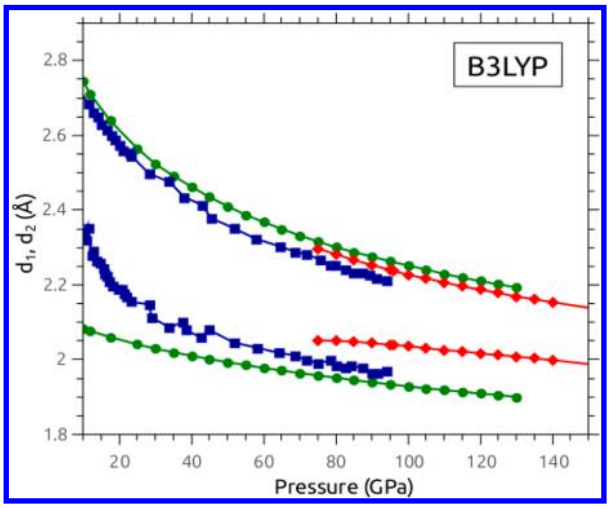

Figure 7. Intermolecular B3LYP d_1 (lower curve) and d_2 (upper curve) distances vs experimental data from ref 4. ε data (green), ζ data (red), and experimental results in blue from ref 7.

the experimental data of ref 4. Note that the agreement with experimental results improves at higher pressures.

Figure 8 shows the evolution of the unit cell volume with pressure. Note the excellent agreement of the B3LYP predicted values with experimental data and the better performance of the hybrid method in comparison with the previous GGA results from ref 12. We stress that in this case the agreement with experiment is nearly pressure-independent and this fact can be simply explained: since the $a(b)$ cell parameters are slightly over(under)-estimated, their β angle-weighted product with the very accurate theoretical c parameter leads to an effective cancellation of these errors.

Table 1 summarizes the results obtained with the methods explored here. The wide range of transition pressures obtained with the various schemes gives rise to many theoretical and methodological questions, notably those related to the role played by the inclusion of the non-local HF exchange through the use of hybrid-type functionals. Note that while the HF method does not predict the appearance of the ζ phase at all, LDA and GGA-type approaches yield too low transition pressures, in agreement with previous results obtained using these methods with plane wave basis sets (ref 20). It is also

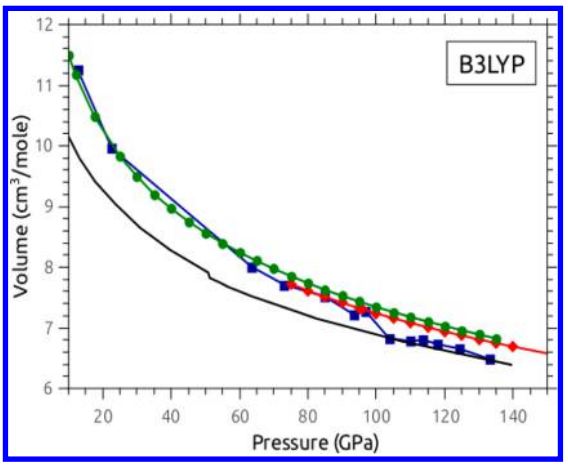

Figure 8. $(O_2)_4$ unit cell volume vs pressure at the B3LYP level. Previous theoretical prediction at the PBE/PW level (black curve) from ref 12. ε data (green), ζ data (red), and experimental results in blue from ref 7.

Table 1. ε−ζ Transition Pressures and Coexistence Ranges Obtained with the Various Methods

	pressure (GPa)	% of HF exchange
HF	no transition up to 160	100
LDA	25, no phase coexistence	
GGA		
BLYP	30, no phase coexistence	
SOGGAXC	25, phase coexistence 25−35	
PBE	30, phase coexistence 30−45 (50)[a]	
B88PW91	30, phase coexistence 30−50	
Meta-GGA		
M06-L	10, phase coexistence 10−25	
Hybrid		
M06	80, phase coexistence 80−120	27
PBE0	85, phase coexistence 85−155	25
B3PW91	75, phase coexistence 75−145	20
B3LYP	75, phase coexistence 75−135	20
Experiment[b]	95, phase coexistence 95−110	

[a]From ref 13 with the PW basis set. [b]Exp. from ref 7.

interesting to note that two functionals of the same family, M06 and M06-L, lead to such different performance: the former, a hybrid method including 27% of non-local HF exchange, predicts a 80−120 GPa phase coexistence region, while the second (a meta-GGA method without HF exchange) yields a worse prediction than most GGA methods (a too low transition pressure ca. 10 GPa).

However, an interesting fact is that the amount of non-local HF exchange critically determines the phase coexistence range, lower fractions of HF exchange yielding lower-pressure phase coexistence regimes. Indeed, while PBE0 has only 5% more HF exchange than B3PW91 or B3LYP (both including 20% of HF exchange), these hybrid functionals lead to quantitatively different results. PBE0 predicts the appearance of the ζ phase at 85 GPa and the persistence of the ε phase up to ca. 160 GPa, while the B3PW91/B3LYP approaches predict the appearance of the ζ phase at 75 GPa but the ε phase disappears at lower pressure ca. 135 GPa. This is a particularly important result since it reveals that a precise (delicate) coupling of the exchange contributions (local plus non-local parts) is necessary. Note that the PBE0 prediction of the onset of the phase

DOI: 10.1021/acs.jctc.5b00017
J. Chem. Theory Comput. XXXX, XXX, XXX−XXX

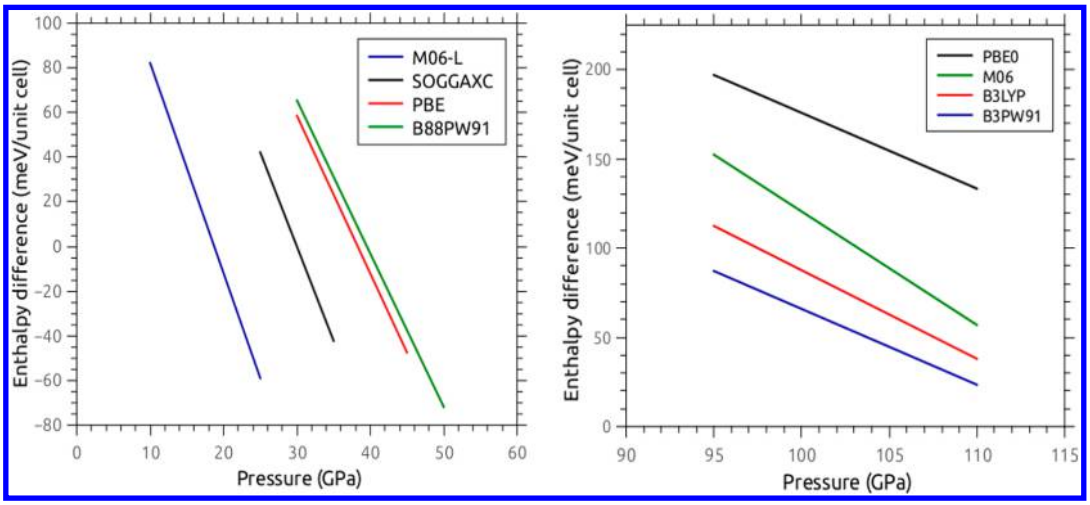

Figure 9. Enthalpy difference in the phase coexistence region vs pressure. The ϵ phase is the reference at each pressure. GGA functionals (left), hybrid functionals (right).

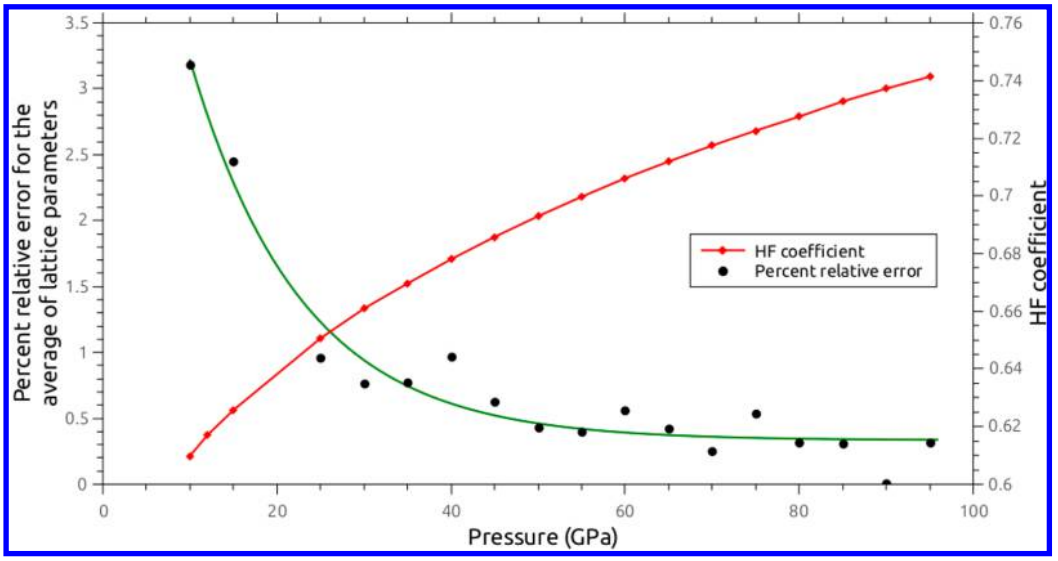

Figure 10. Evolution of the RMS percent error of the B3LYP ϵ lattice parameters and the HF coefficient in the CASSCF(8,8) wave function of the $(O_2)_4$ unit cell vs pressure.

coexistence range is the one closest to the experimental value of 95 GPa. As we shall see in the following section, the hybrid functional structural predictions are in excellent agreement with the XRD data[4,7] apparently due to a serendipitous cancellation of exchange and correlation errors.

Figure 9 shows the evolution of the enthalpy difference in the phase coexistence region for the ensemble of GGA and hybrid-type functionals explored here. Two important facts can be noted in that figure. First, GGA functionals systematically predict a greater stability of the ζ phase at lower pressures than those predicted by the hybrid functionals. Second, while for the GGA functionals the isoenthalpic condition for both phases is reached at very low pressures (20−40 GPa), for all the hybrid functionals the ζ phase never reaches a lower enthalpy than the ϵ phase, even at very high pressures above the experimental phase coexistence region. Nevertheless we stress that, in purely enthalpic terms, at the B3LYP level and 110 GPa, the ϵ phase is only 38 meV/unit cell more stable than the ζ phase. However, the crucial relative stability issue is out of the scope of the present work and has been properly addressed elsewhere in terms of the Gibbs free energy difference by including the phononic and finite temperature entropic contributions (for details, see section IV below).

C. Evolution of the Multiconfigurational Character of the Wave Function vs Pressure. From the figures presented in the previous section it is interesting to note that the agreement of the hybrid functional results, in particular the d_1 and d_2 intermolecular distances, with the corresponding experimental data, improves as pressure increases. This suggests that the quality of the Kohn−Sham description at the hybrid level of the unit cell improves with pressure. In order to understand why this is so, we performed molecular CASSCF/aug-cc-pVTZ calculations of the cuboid $(O_2)_4$ cluster with eight electrons in eight active orbitals using the B3LYP optimized unit cell geometry at each pressure. This is a CASSCF(8,8) calculation with two π_g orbitals from each O_2 molecule in the optimized unit cell with incremental steps of 10 GPa. For these calculations we used the Molpro-2010 code[33] and the D_{2h} point group for the cuboid $(O_2)_4$ cluster. We recall that the singlet CASSCF(8,8) wave function of the unit cell contains 1252 configuration state functions (CSF). As pointed out before,[30−32] the wave function is strongly multiconfigurational

DOI: 10.1021/acs.jctc.5b00017
J. Chem. Theory Comput. XXXX, XXX, XXX−XXX

at the zero-pressure $(O_2)_4$ optimized geometry but, as the intermolecular distance decreases with pressure, the system becomes better described by single configuration methods. In order to illustrate the correlation of the decreasing multiconfigurational character of the unit cell wave function with the improvement of the structural description for the ε phase with increasing pressure, Figure 10 shows the RMS error of the B3LYP lattice parameters with respect to the experimental values and the HF coefficient in the CASSCF(8,8) wave function at each pressure. It can be seen that the RMS error drops from 3.2% at 10 GPa to less than 0.38% at 95 GPa, while, at the same time, the HF coefficient in the CASSCF wave function grows from 0.61 to 0.74. Table 2 shows the main configurations and their coefficients in the CASSCF(8,8) wave function of the $(O_2)_4$ unit cell at 95 GPa. Note that, even at such a high pressure, 46% of the unit cell wave function is diluted in more than 1000 CSFs at the CASSCF(8,8) level of theory.

Table 2. Main Configurations in Second Quantized Form and Their Coefficients in the CASSCF(8,8) Wavefunction of the Optimized Cuboid $(O_2)_4$ Unit Cell at 95 GPa[a]

configuration	coefficient
20 20 20 20	0.7413081
20 20 02 20	−0.1462290
20 02 20 20	−0.1462290
20 20 20 02	−0.1003274
20 20 bb aa	−0.0989988
20 20 aa bb	−0.0989988
20 bb 20 aa	0.0989988
20 aa 20 bb	0.0989988
02 20 20 20	−0.0987868
bb 20 aa 20	−0.0970320
aa 20 bb 20	−0.0970320
bb aa 20 20	0.0970320
aa bb 20 20	0.0970320
20 20 ba ab	0.0875484

[a]Occupation numbers in each column correspond to the B_{3u}, B_{1g}, B_{2g}, and A_u irreps of the D_{2h} group.

Since strong nondynamical correlation effects in the $(O_2)_4$ unit cell are still present even at such high pressure, it is clear that the good performance of single-reference hybrid functional DFT methods is due to a lucky cancellation of errors between the exchange and the correlation parts of these hybrid functionals. However, periodic HF (also a single reference method) does not predict the phase transition at all because both dynamic and nondynamic correlation effects are crucial and completely missing at this level of theory. The PBE, LYP, and PW91 correlation functionals, when combined with a small amount (20−25%) of non-local HF exchange, seem to recover these effects in a quite effective manner, especially at the highest pressures.

D. Evolution of the Electronic Structure with Pressure.

In order to study the evolution of the electronic structure, we have obtained the band structure of the ε phase from 10 to 135 GPa and for the ζ phase from 75 to 160 GPa. We present in Figure 11 the B3LYP band structure of both phases at 75 GPa (the lower end of the coexistence regime) while, in Figure 12, we show those obtained at 110 GPa which corresponds to the highest pressure where both phases have experimentally been detected. For clarity we present only the four highest valence bands and the four lowest conduction bands in each case.

Two facts can be seen in Figure 11: first, that the ε band gap is not direct, going from Γ to Y (1/2, 1/2, 0). Second, at the B3LYP level of theory, the ζ phase is already a conductor at 75 GPa.

We found that the band gap of the ε phase exhibits an exponential decrease with pressure, see Figure 13. Note that the band gap is already 2 eV at 15 GPa and that a spectacular 20-fold collapse occurs when the pressure reaches 135 GPa. In Figure 13 we also plot the evolution of the intercell O_2−O_2 intermolecular distance (d_2) and the strong correlation of both curves reveals that the passage from the non-conducting to conducting character is closely related to the structural changes induced by the applied pressure for the ε phase.

We stress that the structural modifications only occur in the *ab* plane, and, accordingly, the electronic changes associated with the conductivity transition are due to a large decrease of the monoelectronic energy of the lowest conduction band at the $Y = (1/2, 1/2, 0)$ point in reciprocal space. However, while

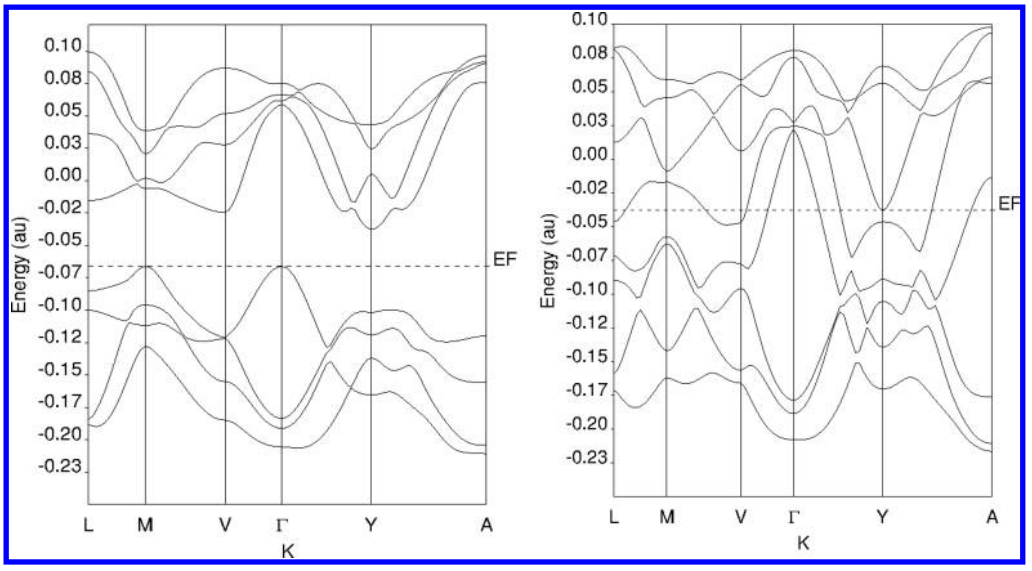

Figure 11. Band structure of the ε (left) and ζ (right) phases at 75 GPa. Fermi level at EF.

DOI: 10.1021/acs.jctc.5b00017
J. Chem. Theory Comput. XXXX, XXX, XXX−XXX

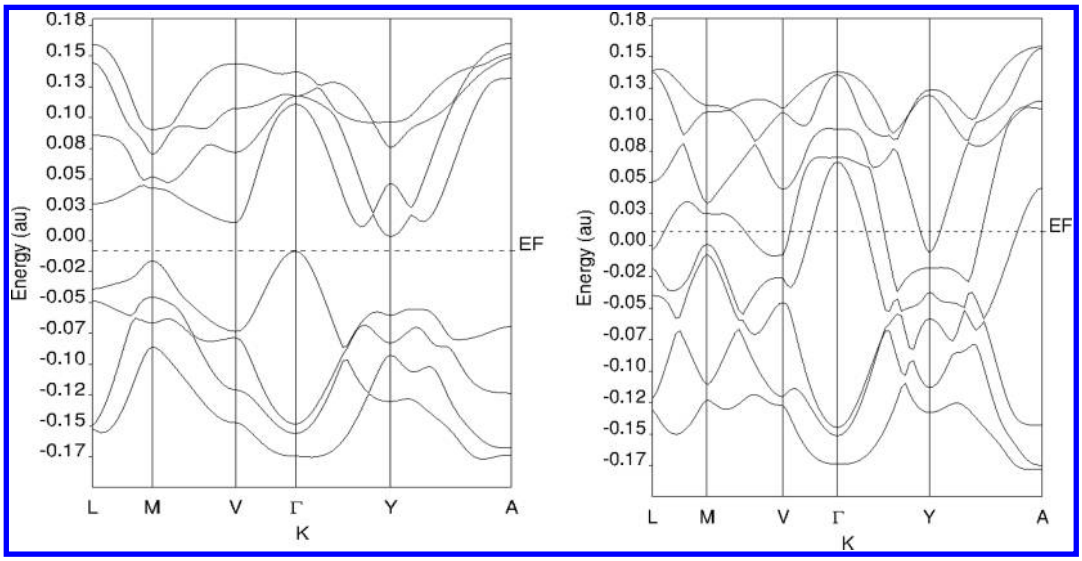

Figure 12. Band structure of the ε (left) and ζ (right) phases at 110 GPa. Fermi level at EF.

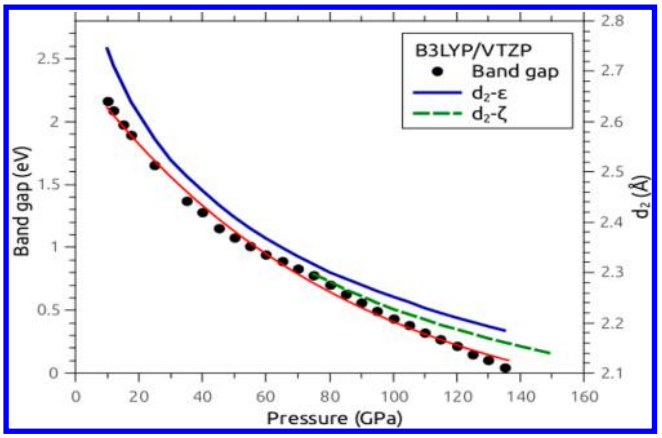

Figure 13. Evolution of the B3LYP ε band gap and intercell distance (d_2) with pressure; the red curve is an exponential fit to the band gap.

experimentally a phase coexistence region has been confirmed between 96 and 110 GPa, the non-conducting to conducting transition has been observed to occur ca. 96 GPa.[7] This suggests that the onset of conductivity is actually related to the appearance of domains of the ζ phase in the diamond-anvil cell experiments. In this direction, it has been hypothesized that the conducting character of the ζ phase can be explained in terms of an increasing overlap of the π_g orbitals of neighboring O_2 molecules[12] that leads to chemical bonding between O_2 molecules of different unit cells as pressure increases. However, this has never been explicitly shown. The strength of chemical bonding can now be quantitatively measured with the electron pair localization function (EPLF)[34] derived from wave function calculations using the following formula[35]

$$\mathrm{EPLF}(r) = \frac{d_{\sigma\sigma}(r) - d_{\sigma\bar{\sigma}}(r)}{d_{\sigma\sigma}(r) + d_{\sigma\bar{\sigma}}(r)}$$

where the shortest spin-like and spin-unlike electron−electron distances are

$$d_{\sigma\sigma}(r) = \sqrt{-\frac{1}{\gamma(r)}\ln\langle\Psi|\sum_{i=1}^{N}\delta(r-r_i)\sum_{j\neq i;\sigma_i=\sigma_j}^{N} e^{-r(r)|r_i-r_j|^2}|\Psi\rangle}$$

$$d_{\sigma\bar{\sigma}}(r) = \sqrt{-\frac{1}{\gamma(r)}\ln\langle\Psi|\sum_{i=1}^{N}\delta(r-r_i)\sum_{j;\sigma_i\neq\sigma_j}^{N} e^{-r(r)|r_i-r_j|^2}|\Psi\rangle}$$

The EPLF is a scalar function in ordinary 3D-space, measuring the localization of electron *pairs*. The EPLF varies from −1 to +1, and it gives a local indicator of electron pairing as follows. In regions of space where electrons are unpaired the average shortest distance between spin-like and spin-unlike electrons are similar, and the EPLF goes to zero (i.e., the homogeneous electron gas). In regions where antiparallel-spin electrons are paired, EPLF takes positive values, and when parallel-spin electrons are paired, the EPLF takes negative values. We have successfully used this approach to study the bonding in tetraoxygen.[36] Here, in order to investigate the presence or absence of chemical bonding between different-unit cell O_2 molecules, we have obtained the EPLF for the singlet state B3LYP/6-311G* wave function for a nine (3 × 3) unit cell molecular model in the *ab* plane for both phases at 100 GPa. Figure 14 shows the EPLF isosurfaces at 0.092 for both

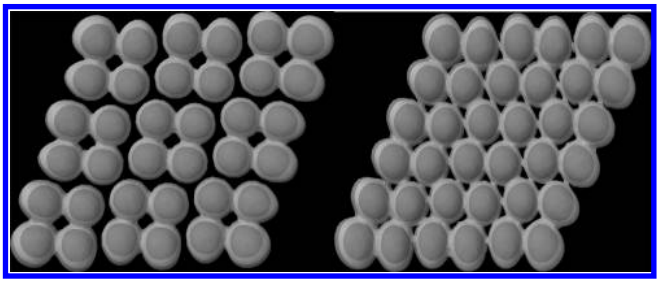

Figure 14. EPLF isosurfaces (0.092) in the *ab* plane for the optimized ε (left) and ζ (right) phases at 100 GPa. Note the clear chemical bonding between different unit cell O_2 molecules for the ζ phase.

phases. The O_2 molecular axis are perpendicular to the page. These figures show that while only the four molecules of the same unit cell for the ε phase are chemically linked together at EPLF = 0.092, the ζ EPLF isosurface already comprises molecules belonging to different unit cells. As suggested by Militzer and Hemley,[14] this intercell chemical bonding can now

DOI: 10.1021/acs.jctc.5b00017
J. Chem. Theory Comput. XXXX, XXX, XXX−XXX

be associated with the conducting character of the ζ phase starting at ca. 100 GPa.

E. Spin-Polarized Description for the ε Phase at Low Pressures. Finally, we note in passing that, at low temperatures, the low-pressure antiferromagnetic phases below 8 GPa where O_2 molecules have spin $S = 1$ are followed by the broad non-magnetic ε phase from about 8 to 96 GPa. According to accurate XRD data,[4,5] in the ε phase O_2 molecules group to form $(O_2)_4$ unit cells while switching to spin $S = 0$. A recent theoretical study by Crespo et al.[38] using the semiempiric DFT +U method as a means to correct the self-interaction error suggests that this is true only above 20 GPa, whereas the $S = 1$ molecular O_2 state survives up to about 20 GPa. However, they also stress that the pressure range where the $S = 1$ molecular O_2 state is more stable than the $S = 0$ state is strongly dependent on the choice of the U parameter (0.8, 1.0, 1.5, or 2 eV); this is so up to 17.6 GPa with $U = 0.8$ eV, but this critical pressure grows to 30 GPa if they use $U = 2$ eV. Using a U parameter fixed at 1 eV they find good agreement with vibrational data,[39,40] but the quality of the structural description cannot be assessed since they did not provide the evolution of the unit cell parameters as functions of U. Based on their semiempiric DFT +U results, these authors suggest that the ε phase thus breaks up into two: a spinless $\varepsilon 0$ (20−96 GPa) and another $\varepsilon 1$ low-pressure phase (8−20 GPa) where the molecules have $S = 1$ but possess only short-range antiferromagnetic correlations. We also point out that their spin-polarized solution yields an artificial broken-symmetry structure, in contradiction with the experimental results where no long-range order has been found for the ε phase at any pressure.

In this direction we have also started to address the possibility of using spin-polarized hybrid functional descriptions, in particular with the B3LYP functional, to study the structural and energetic properties of the ε phase at low pressures. However, we note that our spin-polarized antiferromagnetic enthalpy-driven optimizations yield structures where two molecules possess positive m_s and two (diagonally opposite) possess negative m_s; for instance, we find that at 30 GPa the spin per molecule is still surprisingly large, $S = 0.85$. In agreement with the results of Crespo et al. we also find that the spin-polarized solution has a lower enthalpy than the corresponding spin-unpolarized solution and that the enthalpy difference becomes smaller with increasing pressure. However, with the hybrid B3LYP approach, the spin-polarized solution is dramatically favored (ca. 250 meV/molecule, even at pressures above 30 GPa) but leads also to a broken-symmetry triclinic structure. Nevertheless, quite disappointingly, for spin-polarized solutions the optimized unit cell parameters at pressures below 30 GPa more closely resemble those corresponding to the δ phase, perhaps emphasizing the inadequacy of this single-reference approach at low pressures. A full report will present the results and a thorough discussion of these matters in light of the concepts presented in the "Electronic structure problem" section III-A.

IV. CONCLUSIONS AND PERSPECTIVES

Using several periodic electronic structure methods with localized atomic basis sets, we have addressed the evolution of the structural and electronic parameters of the ε and ζ phases of solid oxygen and compared the results with accurate experimental information. The $(O_2)_4$ unit cell geometries were optimized for both phases imposing the experimental $C2/m$ crystal symmetry. The periodic Hartree−Fock method does not predict the $\varepsilon \rightarrow \zeta$ phase transition up to 160 GPa. In the DFT framework, while the Local Density approximation and Generalized Gradient approximation methods systematically predict too low transition pressures, the performance of hybrid functional methods is dependent on the amount of non-local HF exchange. We found that both GGA and hybrid methods predict a phase coexistence pressure range; however, in many cases, appropriate initial unit cell parameters and density matrix must be used to obtain convergence to the ζ phase at higher pressures. While GGA methods yield too low transition pressures, hybrid approaches lead to phase coexistence ranges in much better agreement with experimental data. PBE0, B3PW91, and B3LYP functionals yield structural parameters (unit cell lengths and intermolecular distances) of both phases that are in excellent accordance with experiments.

From a general standpoint, the present theoretical results on the high-pressure solid phases of oxygen give rise to many questions and new research lines. While from the practical point of view we have found that hybrid DFT approaches yield accurate descriptions of the solid oxygen ε−ζ phase transition, we have explicitly shown that these single-reference methods yield lesser quality results at lower pressures since the unit cell wave function has a stronger multireference character. In this sense the present results raise several questions, notably, why do single-reference based DFT hybrid approaches yield such good quantitative results. In this direction we believe that using the accurate experimental phase coexistence data it might be possible to fine-tune the amount of HF exchange to obtain the best hybrid XC functional for this complex case where the accurate treatment of both dynamical and nondynamical correlation effects is paramount.

As mentioned above, the relative stability of the phases vs pressure, a crucial issue in the context of phase transitions, has been thoroughly presented and discussed elsewhere.[37] In that study it was shown that the purely enthalpic description is not enough to explain the phase transition since the ε phase is still 38 meV/unit cell more stable (at the B3LYP level) than the ζ phase at 110 GPa. Therefore, in order to obtain an accurate Gibbs free energy difference, we included the vibrational thermal and entropic effects at room temperature through phonon calculations on a very large $(O_2)_{64}$ supercell at 110 GPa. Those calculations confirmed that thermal and entropic effects are actually crucial to explain the greater stability of the ζ phase at 110 GPa. Quite remarkably, the phonon calculations led to the discovery that the $C2/m$ structure of the ζ phase is actually a transition state. By following the imaginary ($191i$ cm^{-1}) phononic mode at 110 GPa, we found that the true minimum enthalpy corresponds to a broken symmetry $P1$ $(O_2)_{16}$ supercell. This $P1$ minimum lies 26 meV/unit cell (302 K) lower than the $C2/m$ transition state. The important conclusion derived from that study is that, since the imaginary phononic mode has inversion symmetry, the $C2/m$ $(O_2)_4$ unit cell found for the ζ phase in the XRD experiments at room temperature actually arises as a time-average of symmetrically located $P1$ minima in the $(O_2)_{16}$ supercell potential energy surface.[37]

Finally, we conclude by pointing out that many important issues will be addressed in future studies, such as the possibility of using spin-polarized DFT methods to describe the structure of these high pressure non-magnetic phases, the use of variable non-local HF exchange in the hybrid functionals to fine-tune the structural and energetic properties (in particular to correctly describe the phase coexistence region), and in-depth

DOI: 10.1021/acs.jctc.5b00017
J. Chem. Theory Comput. XXXX, XXX, XXX−XXX

investigation of the electron−phonon coupling which is at the root of the superconducting behavior of the ζ phase near 1 K.

AUTHOR INFORMATION

Corresponding Author

*E-mail: alex@uaem.mx.

Notes

The authors declare no competing financial interest.

ACKNOWLEDGMENTS

A.J.O.C. thanks CONACYT for a graduate scholarship at FC-UAEM. C.Z.W., R.H.L., and A.R.S. thank CONACYT through projects No. 178853, 167921, and 130931, respectively.

REFERENCES

(1) Freiman, Y. A.; Jodl, H. J. *Phys. Rep.* **2004**, *401*, 1.
(2) Akahama, Y.; Kawamura, H.; Shimomura, O. *Phys. Rev. B* **2001**, *64*, 054105.
(3) Akahama, Y.; Kawamura, H.; Häusermann, D.; Hanfland, M.; Shimomura, O. *Phys. Rev. Lett.* **1995**, *74*, 4690.
(4) Fujihisa, H.; Akahama, Y.; Kawamura, H.; Ohishi, Y.; Shimomura, O.; Yamawaki, H.; Sakashita, M.; Gotoh, Y.; Takeya, S.; Honda, K. *Phys. Rev. Lett.* **2006**, *97*, 085503.
(5) Lundergaard, L. F.; Weck, G.; McMahon, M. I.; Desgreniers, S.; Loubeyre, P. *Nature* **2006**, *443*, 201.
(6) Shimizu, K.; Suhara, K.; Ikumo, M.; Eremets, M. I.; Amaya, K. *Nature (London)* **1998**, *393*, 767.
(7) Weck, G.; Desgreniers, S.; Loubeyre, P.; Mezouar, M. *Phys. Rev. Lett.* **2009**, *102*, 255503.
(8) Goncharov, A. F.; Gregoryans, E.; Hemley, R. J.; Mao, H. *Phys. Rev. B* **2003**, *68*, 100.
(9) Serra, S.; Chiarotti, G.; Scandolo, S.; Tosatti, E. *Phys. Rev. Lett.* **1998**, *80*, 5160.
(10) Neaton, J. B.; Ashcroft, N. W. *Phys. Rev. Lett.* **2002**, *88*, 205503.
(11) Oganov, A. R.; Glass, C. W. *J. Chem. Phys.* **2006**, *124*, 244704.
(12) Ma, Y.; Oganov, A. R.; Glass, C. W. *Phys. Rev. B* **2007**, *76*, 064101.
(13) Kim, D. Y.; Lebègue, S.; Moysés Araújo, C.; Arnaud, B.; Alouani, M.; Ahuja, R. *Phys. Rev. B* **2008**, *77*, 092104.
(14) Militzer, B.; Hemley, R. J. *Nature* **2006**, *443*, 150.
(15) Dovesi, R.; Orlando, R.; Erba, A.; Zicovich-Wilson, C. M.; Civalleri, B.; Casassa, S.; Maschio, L.; Ferrabone, M.; De La Pierre, M.; D'Arco, P.; Noël, Y.; Causà, M.; Rérat, M.; Kirtman, B. CRYSTAL14: A program for the ab *initio* investigation of crystalline solids. *Int. J. Quantum Chem.* **2014**, *114*, 1287 see http://www.crystal.unito.it.
(16) (a) Zicovich-Wilson, C. M.; Kirtman, B.; Civalleri, B.; Ramírez-Solís, A. *Phys. Chem. Chem. Phys.* **2010**, *12*, 3289. (b) Dovesi, R.; Orlando, R.; Erba, A.; Zicovich-Wilson, C. M.; Civalleri, B.; Casassa, S.; Maschio, L.; Ferrabone, M.; De La Pierre, M.; D'Arco, P.; Noël, Y.; Causà, M.; Rérat, M.; Kirtman, B. *Int. J. Quantum Chem.* **2014**, *114*, 1287. (c) Zicovich-Wilson, C. M.; Pascale, F.; Roetti, C.; Saunders, V. R.; Orlando, R.; Dovesi, R. *J. Comput. Chem.* **2004**, *25*, 1873.
(17) Perdew, J. P.; Wang, Y. *Phys. Rev. B* **1992**, *45* (45), 13244.
(18) Becke, A. D. *Phys. Rev. A* **1988**, *38*, 3098.
(19) Lee, C.; Yang, W.; Parr, R. G. *Phys. Rev. B* **1988**, *37*, 785.
(20) Perdew, J. P.; Burke, K.; Ernzerhof, M. *Phys. Rev. Lett.* **1996**, *77*, 3865.
(21) Zhao, Y.; Truhlar, D. G. *J. Chem. Phys.* **2008**, *128*, 184109.
(22) Perdew, J. P.; Chevary, J. A.; Vosko, S. H.; Jackson, K. A.; Pederson, M. R.; Singh, D. J.; Fiolhais, C. *Phys. Rev. B* **1992**, *46*, 6671.
(23) Zhao, Y.; Truhlar, D. G. *J. Chem. Phys.* **2006**, *125*, 194101.
(24) Adamo, C.; Barone, V. *J. Chem. Phys.* **1999**, *110*, 6158.
(25) Zhao, Y.; Truhlar, D. G. *Theor. Chem. Acc.* **2008**, *120*, 215.
(26) Becke, A. D. *J. Chem. Phys.* **1993**, *98*, 5648.
(27) Schäfer, A.; Horn, H.; Ahlrichs, R. *J. Chem. Phys.* **1992**, *97*, 2571.
(28) Broyden, C. G. *Math. Comput.* **1965**, *19*, 577.
(29) Johnson, D. D. *Phys. Rev. B* **1988**, *38*, 12807.
(30) Bartolomei, M.; Carmona-Novillo, E.; Hernández, M. I.; Pérez-Ríos, J.; Campos-Martínez, J.; Hernández-Lamoneda, R. *Phys. Rev. B* **2011**, *84*, 092105.
(31) García-Revilla, M. A.; Francisco, E.; Martín-Pendás, A.; Recio, J. M.; Bartolomei, M.; Hernández, M. I.; Campos-Martínez, J.; Carmona, E.; Hernández-Lamoneda, R. *J. Chem. Theory Comput.* **2013**, *9*, 2179.
(32) Bartolomei, M.; Pérez-Ríos, J.; Carmona-Novillo, E.; Hernández, M. I.; Campos-Martínez, J.; Hernández-Lamoneda, R. *Chem. Phys. Lett.* **2014**, *592*, 170.
(33) Werner, H. J.; Knowles, P. J.; Manby, F. R.; Schütz, M. et al. MOLPRO version 2010.1, a package of *ab initio* programs, 2010; see http://www.molpro.net (accessed Feb 21, 2015).
(34) Scemama, A.; Chaquin, P.; Caffarel, M. *J. Chem. Phys.* **2004**, *121*, 1725.
(35) Scemama, A.; Caffarel, M.; Chaudret, R.; Piquemal, J. P. *J. Chem. Theory Comput.* **2011**, *7*, 618.
(36) Scemama, A.; Caffarel, M.; Ramírez-Solís, A. *J. Phys. Chem. A* **2009**, *113*, 9014.
(37) Ochoa-Calle, A. J.; Zicovich-Wilson, C. M.; Ramírez Solís, A. *Phys. Rev. Lett.* **2015**, submitted for publication.
(38) Crespo, Y.; Fabrizio, M.; Scandolo, S.; Tosatti, E. *Proc. Natl. Acad. Sci.* **2014**, *111*, 10427.
(39) Akahama, Y.; Kawamura, H. *Phys. Rev. B* **1996**, *54*, R15602.
(40) Gorelli, F. A.; Ulivi, L.; Santoro, M.; Bini, R. *Phys. Rev. Lett.* **1999**, *83*, 4093.

DOI: 10.1021/acs.jctc.5b00017
J. Chem. Theory Comput. XXXX, XXX, XXX−XXX